AIAA–2003–3975
On a Non-Reflecting Boundary Condition for Hyperbolic Conservation Laws

Ching Y. Loh
Taitech, Inc.
Beaver Creek, OH

16th AIAA Computational Fluid Dynamics Conference and the 33rd Fluid Dynamics Conference and Exhibit
June 23–26, 2003 / Orlando, FL

ON A NON-REFLECTING BOUNDARY CONDITION FOR HYPERBOLIC CONSERVATION LAWS

Ching Y. Loh*
Taitech Inc.
Beaver Creek, Ohio 44135,USA

Abstract

A non-reflecting boundary condition (NRBC) for practical computations in fluid dynamics and aeroacoustics is presented. The technique is based on the hyperbolicity of the Euler equation system and the first principle of plane (simple) wave propagation [1]. The NRBC is simple and effective, provided the numerical scheme maintains locally a C^1 continuous solution at the boundary. Several numerical examples in 1D, 2D and 3D space are illustrated to demonstrate its robustness in practical computations.

1 Introduction

It is well-known that non-reflecting boundary conditions (NRBCs) play an important role in fluid flow and aeroacoustics computations. The need for artificial boundary conditions arises when the domain of the problem is unbounded and extends to infinity. In order to treat the problem numerically, a domain of finite size is required and artificial boundaries are imposed. At these artificial boundaries, NRBCs are sought for to minimize their influences on the flow. A spurious reflection resulting from an inappropriate numerical boundary condition will contaminate the flow field and may entirely spoil the flow computation. Research on NRBC is a challenging topic in engineering and applied mathematics. For decades, a vast number of papers on NRBC have been published, e.g. see [3-6], the review paper by Givoli [2], and the references cited there.

In one-dimensional flow, at an artificial boundary, Enquist and Majda [3], and Hedstrom [7] proved that a boundary condition is non-reflecting is equivalent to saying that the characteristic variables corresponding to the incoming characteristic curve remain constant across the artificial boundary (see also Hirsch [8], p. 370). For multi-dimensional flow, this 1-D technique is combined with dimension splitting and applied in the practical NRBC treatment. Such a combined treatment has been the topic of many papers on the characteristic based NRBCs (see e.g. [4] and references in [2]).

Other alternative treatments for NRBC found in the literature include (see [2-6]):

(i) in the far-field, using a predictable asymptotic analytical solution at the boundary (the radiation boundary condition),

(ii) diminishing the strength of the waves/disturbances before they reach the artificial boundary, and thus minimizing the reflecting effect. Usually, increased numerical damping is applied to a zone between the core domain and the artificial boundary (the buffer zone or sponge zone) to do the job. In the recently developed PML (perfectly matched layer) method, a specially designed equation system is imposed in the matching layer (or sponge zone) to guarantee the exponential decaying of the disturbances in the layer [5,6].

In the present paper, a different but simple criterion is introduced to treat the NRBCs of the time-dependent hyperbolic conservation laws of gas dynamics. The criterion is based on the first principle of plane (simple) wave propagation [1] rather than the characteristics theory. Emphasis is put on their viable practical applications. As it turns out that the NRBCs used in the recent CE/SE finite volume schemes for flow and aeroacoustics computations (e.g. [14,15]) can be directly derived from this criterion, the present paper also serves to explain why these simple NRBCs of the CE/SE schemes work.

The paper is arranged as follows: In Section 2, based on the hyperbolicity of the Euler equation system and the propagation of plane wave, the continuity criterion of NRBC is introduced and proved. An extrapolation-like NRBC (Type I) based on this criterion and the numerical procedure are described. Then the relation between the NRBC and the flux balance across the boundary surface is established, which leads to another type of NRBC (Type II). In Section 3, several numerical ex-

amples for outflow NRBC in one and multi-dimensional space are presented. Numerical examples with Type II NRBC at the inflow and other artificial boundaries are demonstrated in Section 4. Application of buffer/sponge zones is illustrated in Section 5. At last, the paper is concluded with remarks in Section 6.

As the time-dependent hyperbolic conservation laws of gas dynamics (in dimensionless form) is always incorporated in the new treatments of NRBC in the present paper, they are briefly described here for later use:

$$\boldsymbol{U}_t + \boldsymbol{F}_x + \boldsymbol{G}_y + \boldsymbol{H}_z = \mathbf{Q}, \tag{1}$$

where x, y, z and t are the streamwise and transversal coordinates and time, respectively. The conservative flow variable vector $\boldsymbol{U}$ and the flux vectors in the streamwise and radial directions, $\boldsymbol{F}$, $\boldsymbol{G}$, and $\boldsymbol{H}$, are given by:

$$\boldsymbol{U} = \begin{pmatrix} U_1 \\ U_2 \\ U_3 \\ U_4 \\ U_5 \end{pmatrix} = \begin{pmatrix} \rho \\ \rho u \\ \rho v \\ \rho w \\ \rho e \end{pmatrix}, \boldsymbol{F} = \begin{pmatrix} F_1 \\ F_2 \\ F_3 \\ F_4 \\ F_5 \end{pmatrix} = \begin{pmatrix} \rho u \\ \rho u^2 + p \\ \rho uv \\ \rho uw \\ \rho uH \end{pmatrix},$$

$$\boldsymbol{G} = \begin{pmatrix} G_1 \\ G_2 \\ G_3 \\ G_4 \\ G_5 \end{pmatrix} = \begin{pmatrix} \rho v \\ \rho uv \\ \rho v^2 + p \\ \rho vw \\ \rho vH \end{pmatrix},$$

$$\boldsymbol{H} = \begin{pmatrix} H_1 \\ h_2 \\ H_3 \\ H_4 \\ H_5 \end{pmatrix} = \begin{pmatrix} \rho w \\ \rho wu \\ \rho wv \\ \rho w^2 + p \\ \rho wH \end{pmatrix}.$$

where u, v, w and ρ, p are respectively the velocity components, density and pressure, $e = \frac{p}{\rho(\gamma-1)} + 1/2(u^2 + v^2 + w^2)$, and the enthalpy $H = p/\rho + e$ with $\gamma = 1.4$. The right hand side $\mathbf{Q}$ is the source term which may include the possible external forcing terms and/or viscous fluxes.

By considering (x, y, z, t) as coordinates of a four-dimensional Euclidean space, E_4, and using Gauss's divergence theorem, it follows that Eq. (1) is equivalent to the following integral conservation laws:

$$\oint_{S(V)} \mathbf{I_m} \cdot \mathrm{d}\mathbf{s} = \int_V \mathbf{Q_m} \mathrm{d}V, \qquad m = 1, 2, 3, 4, 5, \tag{2}$$

where $S(V)$ denotes the surface around a volume V in E_4 and $\mathbf{I_m} = (F_m, G_m, H_m, U_m)$ stands for the flux vectors, $\mathbf{I_m} \mathrm{d}\mathbf{s} = \mathbf{I_m} \bullet \mathbf{n} ds$, $\mathbf{n}$ being the outgoing unit normal vector in E_4, is the flux at the infinitesimal surface element ds.

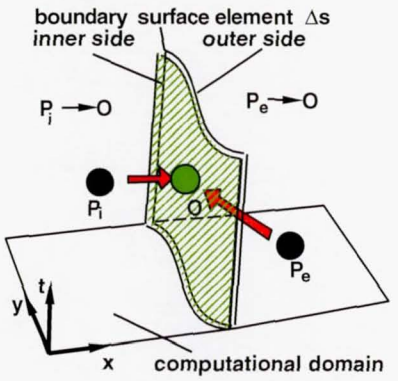

Figure 1: The NRBC criterion in E_3.

2 The continuity criterion of NRBC for time dependent conservation laws

There are various techniques to treat the NRBC based on characteristics theory of the hyperbolic system. For instance, a well-known 1-D flow NRBC treatment by Enquist and Majda [3], and Hedstrom [7] is the requirement that the local perturbation (disturbance) along incoming characteristics be made vanish at the boundary (see [8], p.370). Let $W = (w_1, w_2, w_3)^T$ be the 1-D characteristic flow variables, the above requirement states that for those k such that the corresponding characteristic enters the computational domain through the artificial boundary:

$$\Delta w_k = 0 \tag{3}$$

Thompson [4], for example, has details on the practical implementation of the characteristic NRBCs with a finite difference scheme. Hirsch [8] also offers an excellent resource of various NRBCs.

In finite volume numerical approaches with hyperbolic conservation laws, grid nodes are often cell centers and the boundary faces are often formed by the boundary cell surfaces. No node lies *exactly* on the boundary. As such, a continuity criterion of NRBC and the consequent NRBC treatments are recommended based on the hyperbolicity of the equation system and the first principle of plane wave propagation [1]. They are simple, robust and particularly appropriate for cell center finite volume schemes. Their limitations are also briefly discussed.

2.1 The continuity criterion of NRBC

The continuity criterion is first introduced in an heuristic way and then proved via the first principle of plane wave propagation [1].

Under a general assumption that the flow is continuous near the boundary, i.e., with no shock or contact discontinuity, we first consider the behavior of the characteristic variables $\mathbf{W} = (w_1, w_2, w_3, w_4, w_5)^T$ across the artificial boundary surface element Δs as time elapses. Δs also represents the interface between a boundary cell

and its corresponding ghost cell. Note that any (artificial) spatial boundary is a cylindrical hyper-surface in the space-time E_4 space (Fig. 1 demonstrates the situation in E_3).

Let P_i and P_e be respectively an interior point and an exterior point of the computational domain in the E_4 space. Both P_i and P_e lie in the neighborhood of O, a point on Δs (Fig. 1). Recall the standard NRBC treatment for 1-D flow [3,7],

$$\Delta w_k = w_k(P_i) - w_k(P_e) = 0, \quad for \quad selected \quad k.$$

When P_i tends to O from the interior of the domain and P_e tends to O from the exterior of the domain, the NRBC Eq. (3) becomes:

$$\lim_{P_i \to O} w_k(P_i) = \lim_{P_e \to O} w_k(P_e) = w_k(O) \qquad (4)$$

for those selected ks. Therefore, the usual NRBC treatment is formally interpreted as a continuity problem of w_k across the boundary surface.

Secondly, for the NRBC of multi-dimensional flow, we formally extend the continuity of w_k across the boundary surface to *all* ks rather than just a selected number of ks:

$$\lim_{P_i \to O} w_k(P_i) = \lim_{P_e \to O} w_k(P_e), \quad for \quad all \quad k. \quad (5)$$

Let $\mathbf{U} = (u_1, u_2, u_3, u_4, u_5)^T = (\rho, \rho u, \rho v, \rho w, \rho e)^T$ and $\mathbf{V} = (v_1, v_2, v_3, v_4, v_5)^T = (\rho, u, v, w, p)^T$ be respectively the conservative flow variables and the primitive flow variables. From the local equivalence of the characteristic variables $\mathbf{W}$ and $\mathbf{V}$ or $\mathbf{U}$ (see e.g. Hirsch[8], p.155-156), Eq. (5) is equivalent to the continuity of $\mathbf{V}$ or $\mathbf{U}$ across the artificial boundary surface:

$$\lim_{P_i \to O} u_k(P_i) = \lim_{P_e \to O} u_k(P_e), \quad for \quad all \quad k \qquad (6)$$

or

$$\lim_{P_i \to O} v_k(P_i) = \lim_{P_e \to O} v_k(P_e), \quad for \quad all \quad k \qquad (7)$$

It is advantageous to switch from the continuity relation (5) of $\mathbf{W}$ to that of $\mathbf{V}$ or $\mathbf{U}$, (6) or (7), since the latter can be treated in an easy way. At this stage, the continuity criterion of NRBC is heuristically inferred and will be proved later. The feasibility that *all* u_ks (v_ks and w_ks as well) can be made approximately continuous simultaneously at the boundary surface is demonstrated in the numerical examples of NRBC in § 2.2.1.

Now, with the presence of the artificial boundary s (hyper-surface), E_4 is bisected into two portions, domain interior D_i and domain exterior D_e. Within each portion, the flow is governed by the same Eq. (1). From the first principle of plane wave propagation, it can be shown that

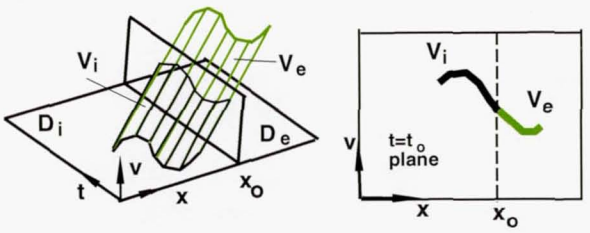

Figure 2: Sketch of the continuity criterion in 1-D flow, only a real component of $\mathbf{V}$ is shown.

locally there is no reflection at the artificial boundary surface s if the continuity criterion Eq. (7) (or Eq. (6), or Eq. (5)) is satisfied.

Proof: Consider a non-conservation form of Eq. (1) in primitive variables $\mathbf{V}$:

$$\frac{\partial \mathbf{V}}{\partial t} + \tilde{A}\frac{\partial \mathbf{V}}{\partial x} + \tilde{B}\frac{\partial \mathbf{V}}{\partial y} + \tilde{C}\frac{\partial \mathbf{V}}{\partial z} = \tilde{\mathbf{Q}}, \qquad (8)$$

where $\tilde{A}$, $\tilde{B}$, and $\tilde{C}$ are the jacobian matrices and functions of $\mathbf{V}$. $\tilde{\mathbf{Q}}$ is the source term vector. As a result of the continuity condition (7), an admissible given set of $\mathbf{V}$ at the boundary s may be used as a common boundary condition to solve separately for $\mathbf{V}_i$ and $\mathbf{V}_e$ in their corresponding subdomains D_i and D_e, which are separated by the artificial boundary s. (Note that generally, the admissible $\mathbf{V}$ given at s should be identical to the solution of $\mathbf{V}$ over the entire domain, see Appendix II). Here, $\mathbf{V}_i$ and $\mathbf{V}_e$ are respectively the solutions of (8) in D_i and D_e. Let $\mathbf{V}$ be the solution of (8) over the entire domain. Due to the uniqueness of solution for well-posed initial-boundary value problems (Appendix II), $\mathbf{V}_i$ is identical to $\mathbf{V}$ in D_i and $\mathbf{V}_e$ is identical to $\mathbf{V}$ in D_e. Therefore, in a neighborhood of s, $\mathbf{V}_i$ and $\mathbf{V}_e$ are mutually a continuation of each other across the boundary s and hence there is no reflection (Fig. 2).

To be more specific in terms of plane wave propagation, notice that from the hyperbolicity of the system (8), for any propagation direction $\mathbf{k} = (k_x, k_y, k_z)$ (the wave number vector) , the matrix $\tilde{K} = k_x\tilde{A} + k_y\tilde{B} + k_z\tilde{C}$ has real eigenvalues and linearly independent left eigenvectors, and then, there exists a plane wave (or simple wave) solution:

$$\mathbf{V} = \tilde{\mathbf{V}} e^{i(\mathbf{k}\bullet\mathbf{x} - \omega t)} \qquad (9)$$

where $\mathbf{x} = (x, y, z)$ is the position vector, $i = \sqrt{-1}$, ω is the angular frequency that is related to the eigenvalues via the dispersion relation (see Courant and Hilbert [1], and Hirsch [8], p. 147, 150, and Appendix I). As a wave solution of the hyperbolic system (8) can be locally written as a superposition of the plane wave solutions by Fourier integral (Appendix I), it suffices to consider only the behavior of a single plane wave solution in the form of (9) at the artificial boundary s.

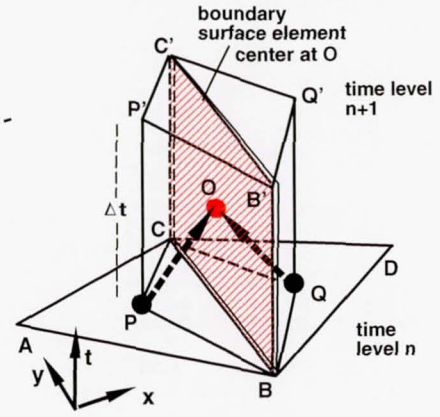

Figure 3: Numerical treatment of NRBC in E_3.

Let O $(\mathbf{x}_o, t_o)$ be any point at the artificial boundary s, then (8) can be locally linearized in the neighborhood of O, i.e.,$\tilde{A}$, $\tilde{B}$ and $\tilde{C}$ are frozen at $\mathbf{V_o}$. For any given wave number vector $\mathbf{k}$, from the continuity criterion (7), $\mathbf{V}_o = \mathbf{V}_i = \mathbf{V}_e$, all $\tilde{A}$, $\tilde{B}$ and $\tilde{C}$ remain the same across the boundary and so also the eigenvalues $\omega_i = \omega_e = \omega$ (see Appendix I). At O, the plane waves $\mathbf{V}_i$ and $\mathbf{V}_e$ share the same $\mathbf{k}$,$\mathbf{x}$, ω and t, and hence the same phase. Again, from the continuity criterion (7), $\mathbf{V}_i = \mathbf{V}_e$, or

$$\tilde{\mathbf{V}}_i e^{i(\mathbf{k}\bullet\mathbf{x}-\omega\ t)} = \tilde{\mathbf{V}}_e e^{i(\mathbf{k}\bullet\mathbf{x}-\omega\ t)},$$

i.e., $\tilde{\mathbf{V}}_i = \tilde{\mathbf{V}}_e$. Thus, the plane waves $\mathbf{V}_i$ and $\mathbf{V}_e$ share the same amplitudes too. Therefore, $\mathbf{V}_i$ is completely identical to $\mathbf{V}_e$ in a neighborhood of O at the boundary (in terms of phase and amplitude), and there is no reflection at O across the artificial boundary surface.

The continuity of $\mathbf{V}$, or $\mathbf{U}$ or $\mathbf{W}$ (Eq.(5)- Eq.(7)) across the boundary surface is thus the basic criterion of NRBC adopted in the present paper. In §2.2, the numerical NRBC (Type I) is constructed based on the continuity criterion. In §2.3, the relation between an NRBC and the flux balance across the boundary surface is established. Such relation leads to another absorbing NRBC (Type II).

2.2 The numerical treatment of NRBC

Fig. 3 illustrates a 2-D (in E_3) NRBC treatment. Let ΔABC be a boundary cell centered at P, with the side BC coincident with the artificial boundary surface. ΔBCD is the ghost cell centered at Q, sharing the boundary edge BC with ΔABC. Let O be the centroid of the boundary surface element $BCC'B'$. The limiting process of $\lim_{P_i \to O} \mathbf{U}(P_i)$ is equivalent to extrapolating $\mathbf{U}$ from the interior node P to O by Taylor expansion. Similarly, $\lim_{P_e \to O} \mathbf{U}(P_e)$ is equivalent to extrapolating $\mathbf{U}$ from the exterior ghost node Q to O by Taylor expansion.

Although theoretically, (6) implies up to C^∞ continuity, in numerical approximation, only low order continuity such as C^0, C^1 or C^2, etc. can be achieved. Since a plane wave solution (9) is based on two parameters, its amplitude and phase, the numerical approximation of $\mathbf{U}$ (or $\mathbf{V}$) is required to be at least C^1 continuous at the artificial boundary in order to be consistent with the physical solution. Taking a 1-D version of (9) for example, the C^1 continuity requirement is explained as follows.

It suffices to consider only a scalar component of $\mathbf{V}$, say, the first one ρ. After discretization, the (artificial) boundary surface element center O is used to represent the entire surface element Δs. Then, from the continuity criterion, approximately, it can be inferred that the 'amplitude' $(\tilde{\rho}_o)_i = (\tilde{\rho}_o)_e = \tilde{\rho}_o$, where the subscripts o, i and e stand respectively for the surface center O, domain interior and exterior. Approximately, at the boundary surface Δs,

$$\rho_i = \tilde{\rho}_o e^{i(k_i x_o - \omega_i t_o)} = \rho_e = \tilde{\rho}_o e^{i(k_e x_o - \omega_e t_o)}. \quad (10)$$

Note that numerically the C^0 continuity result (10) provides no information about the wave number k and the frequency ω. With the presence of phase error, numerical reflection may still occur. However, if the numerical continuity is enhanced from C^0 to C^1, i.e.

$$(\rho_i)_x = ik_i\rho_i = (\rho_e)_x = ik_e\rho_e,$$

$$(\rho_i)_t = -i\omega_i\rho_i = (\rho_e)_t = -i\omega_e\rho_e,$$

then $k_i = k_e$ and $\omega_i = \omega_e$ and there is no phase error.

In constructing the NRBCs, although any one of $\mathbf{U}$, $\mathbf{V}$, and $\mathbf{W}$ can be used, $\mathbf{U}$ is selected since it is employed in the numerical examples in the present paper. Therefore, in addition to $\mathbf{U_p}$, the space and time gradients of $\mathbf{U}$ at P, namely, $\mathbf{U_x}$, $\mathbf{U_y}$, $\mathbf{U_z}$ and $\mathbf{U_t}$ are also required. The resulting linear Taylor expansion (C^1 continuity) yields better accuracy and is consistent with the NRBC criterion. The NRBC at the ghost node Q now turns out to be a problem of how to define $\mathbf{U}$ and its gradients at Q so that the flow is C^1 continuous at the boundary surface (represented by O).

2.2.1 *Examples of NRBC* For the Type I (outflow) NRBC, under a mirror image assumption explained later, it is found that a simple extrapolation technique works well.

First, an example of NRBC in E_3 (2-D space) for triangular mesh is illustrated. As shown in Fig. 3, assume ΔABC is a triangular boundary cell with the edge BC lying on the boundary and conveniently parallel to the y-axis. Define a ghost node D as the mirror image of the triangle vertex A with respect to BC. Then ΔABC and ΔDBC are mutually mirror images of each other (the mirror image assumption). At time step n, conservative

variables $\mathbf{U}$ are given at the cell center P of ΔABC. Then, the NRBC (labeled as Type I) at the geometrical center Q of the ghost cell may be defined as:

$$(\mathbf{U})_Q = (\mathbf{U})_P, (\mathbf{U_x})_Q = (\mathbf{U_x})_P = 0, (\mathbf{U_y})_Q = (\mathbf{U_y})_P. \tag{11}$$

Apply linear Taylor expansions to domain interior and exterior separately:

$$(\mathbf{U}_O)_{interior} = \mathbf{U}_P + (y_O - y_P)(\mathbf{U_y})_P + 1/2\Delta t(\mathbf{U_t})_P.$$

$$(\mathbf{U}_O)_{exterior} = \mathbf{U}_Q + (y_O - y_Q)(\mathbf{U_y})_Q + 1/2\Delta t(\mathbf{U_t})_Q$$

$$hence, \quad (\mathbf{U}_O)_{exterior} = (\mathbf{U}_O)_{interior}.$$

Here, the subscripts P, Q and O of x and y denote the corresponding coordinates of P, Q and O, and from (1), the time partial derivatives $(\mathbf{U_t})_Q = (\mathbf{U_t})_P$ can be directly obtained. Thus, $\mathbf{U}$ is C^1 continuous at O across the boundary surface element, (6) is satisfied and the boundary surface element is non-reflective.

In a consistent way, for 3-D flows, under the same mirror image assumption on the ghost cells, the following extrapolations are valid NRBCs with C^1 continuity:

$$\mathbf{U_Q} = \mathbf{U_p}, (\mathbf{U_x})_\mathbf{Q} = (\mathbf{U_x})_\mathbf{P} = \mathbf{0},$$

$$(\mathbf{U_y})_\mathbf{Q} = (\mathbf{U_y})_\mathbf{P}, (\mathbf{U_z})_\mathbf{Q} = (\mathbf{U_z})_\mathbf{P}, \tag{12}$$

or

$$\mathbf{U_Q} = \mathbf{U_p} + \Delta x(\mathbf{U_x})_\mathbf{P}, (\mathbf{U_x})_\mathbf{Q} = (\mathbf{U_x})_\mathbf{P},$$

$$(\mathbf{U_y})_\mathbf{Q} = (\mathbf{U_y})_\mathbf{P}, (\mathbf{U_z})_\mathbf{Q} = (\mathbf{U_z})_\mathbf{P}, \tag{13}$$

where $\Delta x = x_Q - x_P$.

As demonstrated in the examples in §3 and §4, this Type I NRBC works well for either supersonic or subsonic flows at the outflow boundary, but it should be noted that:

1. (12) or (13) is but a possible selection under the mirror image assumptions, there are other forms of NRBCs based on (5) - (7);

2. The extrapolation technique utilizes the nearby $\mathbf{U}_P$ data to approximate the $\mathbf{U}$ data at the artificial boundary, which is not an unreasonable choice, but there is a danger that the solution could drift away from the true solution (see Appendix II). A remedy is to incorporate the Type I NRBC with other physical boundary conditions (e.g. back pressure, etc.)

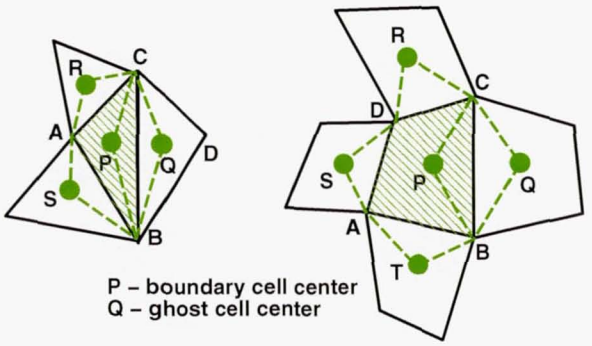

Figure 4: Control volumes (CVs) in E_3 for compact updating. Left: boundary cell ΔABC and the corresponding hexagon CV base $ASBQCRA$; right: quadrilateral boundary cell $ABCD$ and its corresponding octagon CV base $ATBQCRDSA$; R, S, T are centers of neighboring cells and BC the boundary. In any case, quadrilateral $PBQC$ is a portion of the CV base.

2.2.2 *Numerical implementation of NRBC*

The implementation of the NRBC is incorporated in the numerical procedure and may be summarized in the following steps:

(i) Based on the flow data at the boundary cell center P, i.e. $\mathbf{U_P}$ and its spatial gradients (slopes) $\mathbf{U_x}$, $\mathbf{U_y}$ and $\mathbf{U_z}$, determine the flow data $\mathbf{U_Q}$ as well as its gradients $\mathbf{U_x}$, $\mathbf{U_y}$ and $\mathbf{U_z}$, i.e. the NRBC at Q, as described in §2.2.1.

(ii) Update $\mathbf{U}$ at boundary cell center P to the new time level by the conservation laws (2). In order that $\mathbf{U}$ be C^1 continuous across the artificial boundary, the updating procedure must be carefully designed to take account of the accuracy of surface flux calculation. Here a compact updating procedure described in §2.2.3 is recommended.

(iii) After $\mathbf{U}$ at all the interior cell centers of the computational domain are updated, evaluate the new spatial gradients $\mathbf{U_x}$, $\mathbf{U_y}$, $\mathbf{U_z}$ at the boundary cell center P by finite difference. For multi-dimensional flows, a linear equation system is required to solve for the gradients.

(iv) Repeat steps (i) - (iii) and march in time.

2.2.3 *Compact updating* The updating procedure recommended here is identical to the one used in the recent CE/SE method (Chang *et al* [10,11]) and similar to the NT (Nessyahu-Tadmor) scheme [12] in 1-D flow.

The purpose for compact updating is to achieve high accuracy (C^1 continuity) from a small cell stencil (e.g. the stencil formed by the immediate neighboring cells). Therefore, not only $\mathbf{U}$ but also its gradients $\mathbf{U}_x, \mathbf{U}_y$ and $\mathbf{U}_z$ are required. The compact updating is capable of maintaining C^1 continuity of $\mathbf{U}$ across the artificial

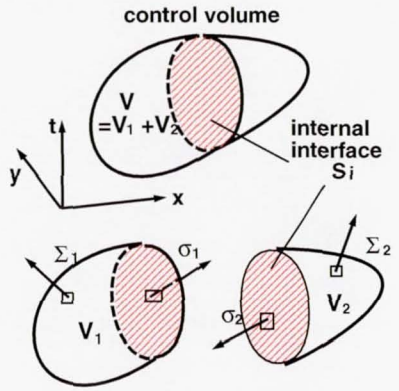

Figure 5: Fluxes balance on an internal face S_i in E_3.

boundary.

Consider a triangular cell ΔABC in E_3 (Fig.4, shaded area). Let P and Q, R, S be respectively the cell centers of ΔABC and its neighboring triangular cells. Most of the finite volume schemes use the space-time cylinder ΔABC as the control volume (CV) for updating $\mathbf{V}$ or $\mathbf{U}$ at P. Surface flux along, say, AB is obtained by extrapolation from S across the cell to the surface center along AB. Another treatment is to include S in the CV and replace the flux along AB by the fluxes along AS and SB. Since S sits right on both surfaces along AS and SB, no extrapolation across the interior of the CV is involved. For the triangular cell ΔABC in Fig. 4 the CV turns out to be a space-time hexagon cylinder in E_3 based on $ASBQCRA$. By applying the integral conservation laws (2) to the CV, updating flow data at P based on the flow data at a *compact* node stencil of Q, R, S is now completed. Fig. 4 also demonstrates that for quadrilateral mesh cells the CV is an octagon cylinder in E_3 (2-D space).

The surface fluxes for the CV surfaces passing through a vertex, say, cell centers Q, R, S, can be evaluated by first extrapolating $\mathbf{U}$ along the surface to their corresponding surface centers by linear Taylor expansion, calculating flux functions $\mathbf{F}$, $\mathbf{G}$ and $\mathbf{H}$, and then incorporating the surface unit normal vector and computing the fluxes. For high space dimensions, the CVs are geometrically more complicated. More details including the updating of $\mathbf{U}_x$, $\mathbf{U}_y$, and $\mathbf{U}_z$ can be found in [10,11].

It should be noted that the compact updating is suggested for boundary cells only. For interior cells, one may still continue to use other finite volume schemes.

2.3 Relation between an NRBC and the flux balance across the boundary surface

In this subsection, the relation between two statements is established. The first one states that the incoming fluxes at the artificial boundary surface are equal to the outgoing fluxes, or fluxes are balanced across the boundary

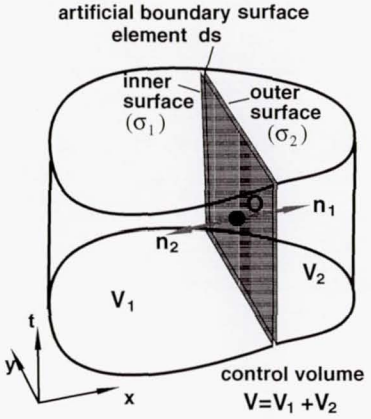

Figure 6: Fluxes balance across a boundary surface element in a control volume (the above figure) in E_3.

surface. Here, the outgoing flux is defined as a portion of the left hand side of (2):

$$\int_{\Delta S} \mathbf{I_m} \cdot \mathrm{d}\mathbf{s}, \qquad m = 1, 2, 3, 4, 5,$$

where ΔS denotes the artificial boundary surface (element). The second statement is that the boundary is non-reflective. Such a relation leads to the Type II NRBC. Numerical implementation of the Type II NRBC is straightforward and will be illustrated in §2.4.

Let V be any control volume in the E_4 space intersected and divided into two portions V_1 and V_2 by an internal surface S_i. Let Σ_1, Σ_2 and σ_1, σ_2 be the fluxes around the surfaces of V_1 and V_2 respectively. Here σ_1 and σ_2 are the outgoing fluxes at the interface S_i for V_1 and V_2 respectively (Fig. 5). Then, the following lemma holds:

Lemma 1: For a control volume V in the E_4 space, fluxes passing through any of its *internal* surface S_i are balanced, i.e. $\sigma_1 + \sigma_2 = 0$.

Proof: Apply (2) to V, V_1 and V_2 separately. We have

$$\Sigma_1 + \Sigma_2 = \int_V \mathbf{Q_m} \mathrm{d}V,$$

$$\Sigma_1 + \sigma_1 = \int_{V_1} \mathbf{Q_m} \mathrm{d}V, \quad \Sigma_2 + \sigma_2 = \int_{V_2} \mathbf{Q_m} \mathrm{d}V.$$

Add the second and the third equations and then subtract the first one, we have $\sigma_1 + \sigma_2 = 0$.

In other words, across any interior surfaces, no extra 'source' should be generated.

Next, we show that locally the continuity of flow variables (Eq. (5), (6) or (7)) can be inferred from flux balance. Hence, flux balance suffices for an NRBC.

Consider an element ds of the cylindrical spatial boundary surface in E_4. As shown in the control volume in Fig. 6 (in E_3), ds is centered at O. Assume the outgoing unit normal vector at O is $\mathbf{n_1} = (n_x, n_y, n_z, 0)^T$, then, the incoming unit normal is $\mathbf{n_2} = (-n_x, -n_y, -n_z, 0)^T$. The outgoing flux $\sigma_\mathbf{1}$ for the inner boundary surface:

$$\sigma_\mathbf{1} = \begin{pmatrix} \sigma_{11} \\ \sigma_{12} \\ \sigma_{13} \\ \sigma_{14} \\ \sigma_{15} \end{pmatrix} = ds[n_x \begin{pmatrix} F_1 \\ F_2 \\ F_3 \\ F_4 \\ F_5 \end{pmatrix} + n_y \begin{pmatrix} G_1 \\ G_2 \\ G_3 \\ G_4 \\ G_5 \end{pmatrix} + n_z \begin{pmatrix} H_1 \\ H_2 \\ H_3 \\ H_4 \\ H_5 \end{pmatrix}]$$

$$= ds[n_x\mathbf{F} + n_y\mathbf{G} + n_z\mathbf{H}].$$

Let the outgoing boundary surface flux vector be:

$$\mathbf{L} = [n_x\mathbf{F} + n_y\mathbf{G} + n_z\mathbf{H}],$$

then

$$\mathbf{L} = \sigma_\mathbf{1}/ds.$$

Let $\mathbf{V} = (\rho, u, v, w, p)^T$ be the primitive flow variable vector. $\mathbf{L}$ may be considered as a non-linear vector function of $\mathbf{V}$. The jacobian matrix $\frac{\partial \mathbf{L}}{\partial \mathbf{V}}$ has the eigen values (e.g. see Hirsch [8], p.177):

$$\lambda_1 = \lambda_2 = \lambda_3 = u \cdot n_x + v \cdot n_y + w \cdot n_z,$$

$$\lambda_4 = \lambda_1 - c, \lambda_5 = \lambda_1 + c.$$

where c is the speed of sound. If none of the eigenvalues vanishes at O, the jacobian $\frac{\partial \mathbf{L}}{\partial \mathbf{V}}$ is non-singular, and an inverse vector function, the primitive flow variables $\mathbf{V}$ as a vector function of the surface flux $\mathbf{L}$ exists. Thus,

Lemma 2: If the jacobian $\frac{\partial \mathbf{L}}{\partial \mathbf{V}}$ is non-singular, then, locally, the primitive variables $\mathbf{V}$ are uniquely defined by the flux vector $\mathbf{L}$ at the center O of ds.

Proof: Assume $\mathbf{L}(\mathbf{V_1}) = \mathbf{L_1}$ and there is another $\mathbf{V_2}$ in the neighborhood of $\mathbf{V_1}$, such that $\mathbf{L}(\mathbf{V_2}) = \mathbf{L_1}$. By a linear Taylor expansion,

$$\mathbf{L}(\mathbf{V_2}) - \mathbf{L}(\mathbf{V_1}) =$$

$$(\frac{\partial \mathbf{L}}{\partial \mathbf{V}})_{\mathbf{V}=\mathbf{V_1}}(\mathbf{V_2} - \mathbf{V_1}) + O(|\mathbf{V_2} - \mathbf{V_1}|^2) = \mathbf{0}$$

Hence $\mathbf{V_2} - \mathbf{V_1} = \mathbf{0}$ or $\mathbf{V_2} = \mathbf{V_1}$ since the first order term cannot cancel with the second order term.

From Lemma 2 and the NRBC continuity criterion (7), it is inferred that locally, under the condition that the jacobian $\frac{\partial \mathbf{L}}{\partial \mathbf{V}}$ is non-singular, the following lemma holds:

Lemma 3: For hyperbolic conservation laws of gas dynamics, an element of the artificial boundary surface is non-reflective if its outgoing fluxes and incoming fluxes are equal (balanced).

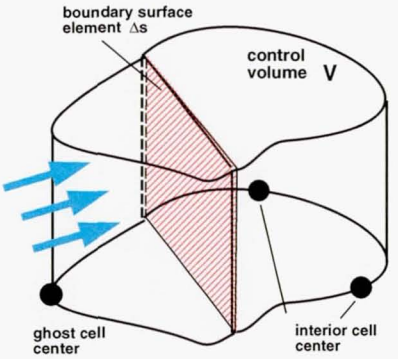

Figure 7: NRBC at inflow in E_3. Inflow data are given at the ghost cell center.

Lemma 3 states that conditionally the flux balance across a boundary surface element is a sufficient condition for NRBC. With the concept of flux balance, there is also an intuitive interpretation of the commonly used terms for NRBC such as 'transparent' and 'absorbing'. If the flux 100% passes through the boundary surface element (or the flux is balanced), the boundary surface is said to be 'transparent' or 'absorbing' to the fluxes. Chang *et al* [9] were the first attempting to explain the 1-D NRBC using flux concepts.

2.4 Implementation of absorbing boundary condition

The lemmas in §2.3 can be easily applied to construct the Type II NRBC. In case that at the ghost cell center nodes flow variables must be specified as the given values (e.g. at the inflow boundary, Fig. 7), another type (Type II) of NRBC - absorbing NRBC arises. A control volume V across the boundary surface is needed to apply the divergence theorem (2). As shown in Fig. 7, the ghost cell center lies outside of the domain, and the boundary surface element Δs is an *internal* surface of the control volume V, then, from Lemma 1 and Lemma 3, Δs is *automatically* a non-reflective boundary surface element.

The Type II NRBC states that no extra condition of NRBC is needed with the prescribed flow boundary conditions at the ghost cell center. This Type II NRBC is flexible and valid with practically any cell shapes or configurations. Ghost cells are not required to be mirror images of the corresponding boundary cells. However, it is noted that $\mathbf{U}$ is still required to be C^1 continuous across the artificial boundary surface. Consequently, the compact updating is still recommended for the Type II NRBC.

In many cases, over a long time period, the (subsonic) flow may develop a flow near the inflow boundary that is different from the imposed boundary conditions, or the boundary condition becomes 'overdetermined', then, a 'matched layer' may be formed between the computed

interior flow and the imposed flow boundary condition (see Fig. 18). The situation is somewhat similar to that in the PML (perfectly matched layer) method [5,6]. The shock-capturing numerical scheme should be able to quickly resolve this non-physical discontinuity in a few cells.

2.5 Discussions on the NRBCs

In practical applications, due to discretization, approximation and lack of information in the domain exterior, there are limitations for both Type I and Type II NRBCs.

For Type I NRBC, as mentioned in §2.2.1, extrapolation technique might lead to drifting or deviation from the true solution because no flow data outside the outflow boundary is available. In addition, under the mirror image assumption on the ghost cells in §2.2.1 and the assumption that the boundary surface Δs is normal to the x axis, the NRBC (12) implies that the NRBC continuity criterion (5 - 7) are satisfied at any point on Δs. However, as explained in the following, due to discretization and the possible consequent phase error, the accuracy of the NRBC could be degraded.

Consider a Fourier mode in the plane wave solution (9): $e^{i(\mathbf{k}\bullet\mathbf{x}-\omega\, t)}$. Here, $\theta(x,t) = \mathbf{k}\bullet\mathbf{x} - \omega t$ is the phase of the wave mode, with $\mathbf{k}$ being the wave number vector in the propagation direction. Generally, the direction of $\mathbf{k}$ may or may not be the same as the flow direction. $\theta(x,t) = const.$ stands for a wavefront (or a characteristic surface, see e.g. Hirsch [8], p.150, Courant and Hilbert [1]). After discretization, the center O of Δs (Fig. 3) is employed to represent the entire Δs. Then how much phase error is introduced to the Fourier mode by the discretization? Let $\mathbf{x} = (x,y,z)$ be the position vector of any point on Δs and $\mathbf{x}_O$ the position vector of the center O. For clarity, assume time t is held unchanged. Then, after discretization, the phase error $\Delta\theta$ due to replacing $\mathbf{x}$ by $\mathbf{x}_O$ is:

$$\Delta\theta = \mathbf{k}\bullet\mathbf{x} - \mathbf{k}\bullet\mathbf{x}_O = \mathbf{k}\bullet(\mathbf{x}-\mathbf{x}_O) \qquad (14)$$

note that $\Delta\mathbf{x} = \mathbf{x} - \mathbf{x}_O$ lies on Δs, $\Delta\theta = 0$ when $\mathbf{k}$ is normal to Δs. Therefore, for Type I NRBC, the best result is obtained when the wave propagation direction is normal or only slightly oblique to the boundary surface. Otherwise, a phase error of order $O(\Delta\mathbf{x})$ may be introduced. It deteriorates the accuracy of NRBC and causes numerical reflection.

For Type II NRBC, in addition to the similar phase error of Type I NRBC, there are other restrictions too. In §2.3, Lemma 3 is conditionally valid because it is based on the one to one correspondence between the boundary surface flux vector $\mathbf{L}$ and the primitive flow variable vector $\mathbf{V}$. The latter relies on the non-singularity of the jacobian $\frac{\partial\mathbf{L}}{\partial\mathbf{V}}$. In case that $\frac{\partial\mathbf{L}}{\partial\mathbf{V}}$ is singular, Lemma 3 may fail. In addition, Lemma 3 is valid only locally. Globally, the relation between $\mathbf{L}$ and $\mathbf{V}$ involves a quadratic equation, the vector function $\mathbf{V}(\mathbf{L})$ could be multi-valued. This could break the one to one correspondence between $\mathbf{L}$ and $\mathbf{V}$ globally and lead to the failure of Lemma 3 in the global sense.

x	EXACT	CE/SE
430.00	0.0000000000	0.0000000000
431.00	0.0000000000	0.0000000000
432.00	0.0000000000	0.0000000000
433.00	0.0000000001	0.0000000001
434.00	0.0000000014	0.0000000014
435.00	0.0000000149	0.0000000149
436.00	0.0000001391	0.0000001391
437.00	0.0000011125	0.0000011125
438.00	0.0000076294	0.0000076294
439.00	0.0000448527	0.0000448527
440.00	0.0002260436	0.0002260436
441.00	0.0009765625	0.0009765625
442.00	0.0036166981	0.0036166981
443.00	0.0114823007	0.0114823007
444.00	0.0312500000	0.0312500000
445.00	0.0729080650	0.0729080650
446.00	0.1458161299	0.1458161299
447.00	0.2500000000	0.2500000000
448.00	0.3674336231	0.3674336231
449.00	0.4629373561	0.4629373561
450.00	0.5000000000	0.5000000000
451.00	0.4629373561	0.4629373561

Figure 8: Comparison of exact and numerical results at the domain boundary for the 1-D Gaussian pulse problem.

In a nutshell, in reality, there are various situations that the Type I or II NRBCs can only be partially or approximately implemented, causing spurious reflections at the (artificial) boundary or deviation from the true solution. In practice, an effective remedy is to impose a buffer/sponge zone between the boundary and the interior domain. Although the same governing equations (1) or (2) are employed in the sponge zone, numerical damping is highly increased to diminish the wave/disturbance amplitude before it reaches the boundary and to minimize the spurious reflection. An example is depicted in §5.

3 Numerical examples for outflow NRBC

In this Section and §4, the effectiveness of these NRBCs is demonstrated in numerical examples in one, two and three dimensional spaces.

In principle, any finite volume scheme can be used with the above NRBC if it can be manipulated at certain high accuracy. Here the recently developed space-time conservation element and solution element (CE/SE) method [10,11] is chosen for computing the examples since the compact updating is a standard procedure in the scheme, making application of the NRBCs straightforward and effective. Full details of the method are described in [10,11]. The Type I NRBCs used with the CE/SE method are identical to (12), with possible minor

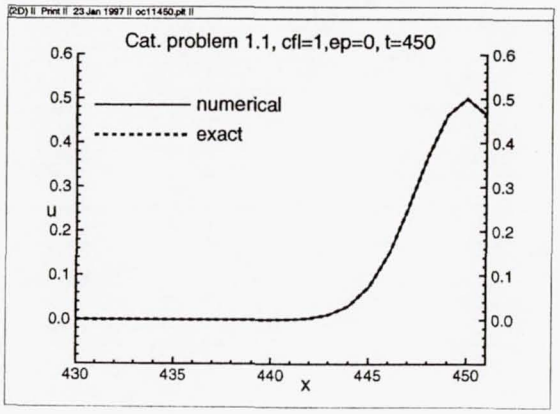

Figure 9: Propagation of 1-D Gaussian pulse at the domain boundary.

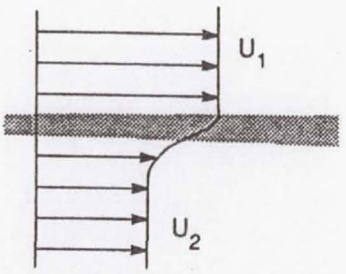

Figure 10: Free shear layer instability problem, $u_1 = U_1 = 1$, $v_1 = 0$, $p_1 = 1/3.15$, $\rho_1 = 1$, $M_1 = 1.5, u_2 = U_2 = .7391\,304$, $v_2 = 0$, $p_2 = 1/3.15, \rho_2 = 0.5405405$, with subscripts $1, 2$ denoting the fast and slow streams respectively.

modification according to the grid layout.

3.1 Propagation of a 1-D Gaussian pulse

Consider a scalar initial value problem:

$$\frac{\partial u}{\partial t} + \frac{\partial u}{\partial x} = 0$$

over the range $-20 \leqslant x \leqslant 450$, with a Gaussian pulse $u = 0.5exp\left[-(ln2)(\frac{x}{3})^2\right]$ at $t = 0$. This is one of the benchmark problems of the 1st CAA Workshop [13](Category 1, Problem 1). The exact solution given there is:

$$u = 0.5exp\left[-(ln2)(\frac{x-t}{3})^2\right].$$

In this example, $\Delta x = 1$ is chosen and $\Delta t = 1$ is based on CFL number $= 1$. With CFL number $= 1$, and other parameters $\epsilon = 0$ and $\alpha = 0$, the CE/SE scheme yields a numerical result which is identical to the exact solution in the *interior* of the domain $-20 \leqslant x \leqslant 451$. Thus, performance of the outflow Type I NRBC at $x = 451$ can be easily validated. At $t = 450$, the Gaussian pulse is passing through the outflow boundary $x = 451$, where the Type I NRBC (12) with appropriate modification to 1-D flow is imposed. The table in Fig. 8 lists the exact solution and the CE/SE result from $x = 430$ to $x = 451$. The result is also plotted in Fig. 9. It is seen that they are completely identical (up to 10 decimal places) and there is absolutely no reflection, although the grid is rather crude with $\Delta x = 1$.

3.2 2-D free shear layer instability and vortex roll-up

The problem considered here is identical to the inviscid free shear layer instability problem considered in [14] (Fig. 10). The background mean flow consists of a fast stream (supersonic) in the upper half domain and a slow stream (subsonic) in the lower half domain. The two parallel streams are connected by a continuously changing shear layer of the hyperbolic tangent profile.

In the test, two computational domains are chosen. The first one is $0 \leqslant x \leqslant 200$ and $-10 \leqslant y \leqslant 10$, with a grid of $200\times$ 100 uniform cells. The second one is $0 \leqslant x \leqslant 100$ and $-10 \leqslant y \leqslant 10$, with a grid of 100×1 00 uniform cells. Both cases have exactly the same grid cell sizes, time step size $\Delta t = 0.15$, and parameters $\epsilon = 0.2$, $\alpha = 0$. They are both run for 4000 time steps when the spatial instability is fully developed. To ensure that the instability waves and vortex roll-up develop quickly, a large perturbation amplitude of 0.02 at the most unstable frequency is chosen for the eigenfunctions. At the outflow boundaries, the Type I outflow NRBC is used. Figure 11 demonstrates snapshots of the isobars and isopycnics in the two cases. These contours are observed to be almost identical to each other in their common domain portion. The contours in the short domain seem as if they were a piece chopped off from the longer one. This shows that the outflow NRBC in this case is nearly perfect.

3.3 Acoustic Pulse Propagation

This problem is a typical subsonic wave propagation problem [13]. The computational domain in the x-y plane is a square with $-100 \leqslant x \leqslant 100$, and $0 \leqslant y \leqslant 200$. A uniform $201\times$ 201 (triangulated) grid is used with $\Delta x = \Delta y = 1$. Initially, a Gaussian acoustic pulse is located at the lower portion of the domain ($x = 0, y = 25$), with a mean flow of Mach number $M = 0.5$ in x direction and a solid wall at the bottom. At the other three boundaries, Type II NRBC is used. By choosing a small amplitude factor $\delta = 0.001$, the Euler equations are practically linearized. Fig. 12 shows the isobars at $t = 100$ and the comparison between numerical and analytical results for density along the line $x = y$ for $0 \leqslant x \leqslant 100$. Although the wave propagation direction is oblique to the

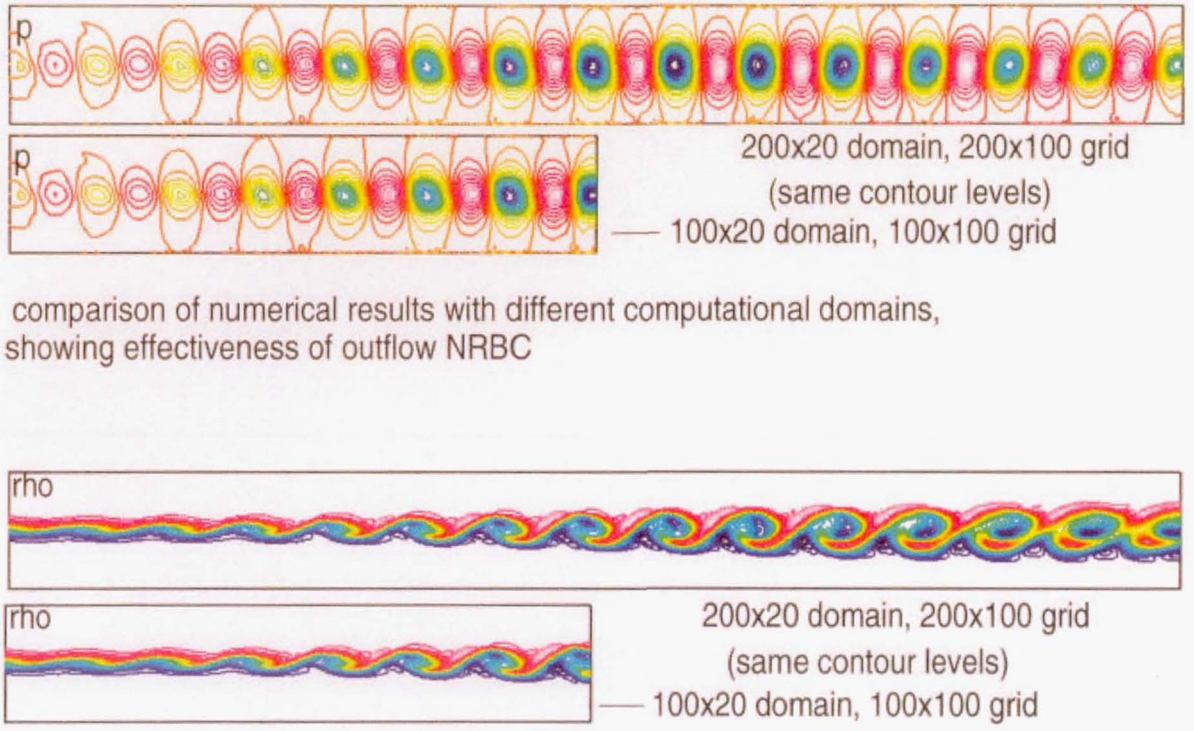

Figure 11: Contours for long and short domains, showing effectiveness of the outflow NRBC.

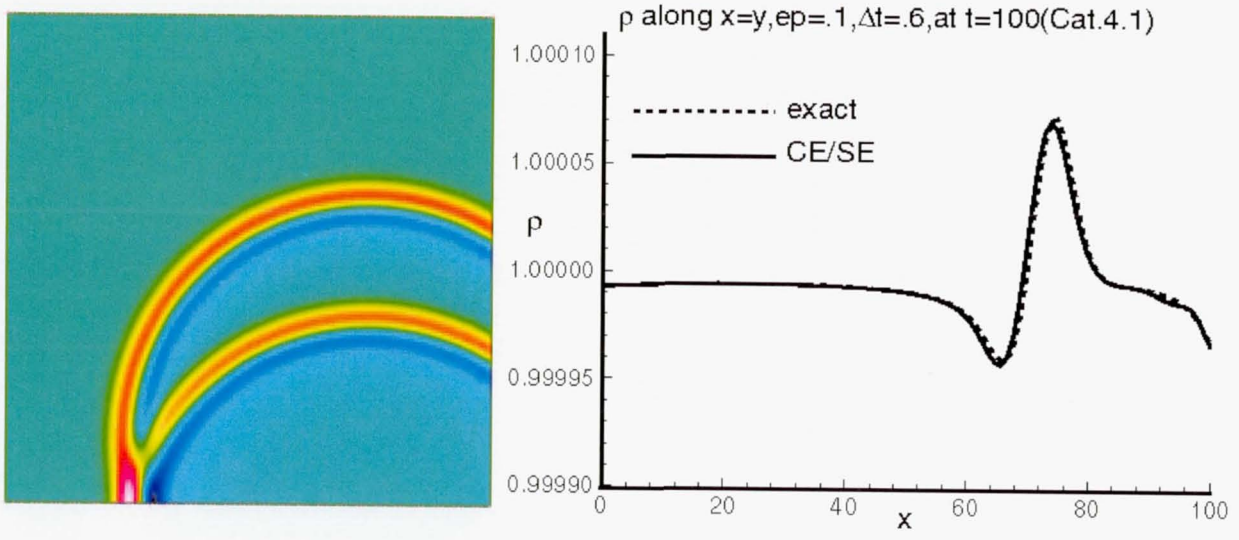

Figure 12: An acoustic pulse above a solid surface passing through the outflow boundary.

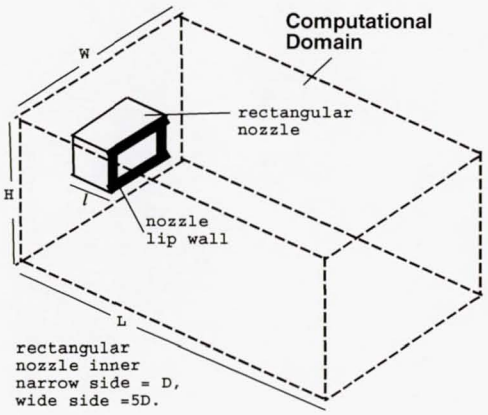

Figure 13: Sketch of the rectangular jet, aspect ratio 5, jet Mach number $M_{\overline{f}}$= 1 .6, $L = 16D, W = 16D$ and $H = 5.6D$.

outflow boundary, only tiny reflection is observed from Fig. 12. Another 2-D example with completely subsonic flow will be illustrated in §4.

3.4 3-D rectangular jet flow

Fig. 13 is the sketch of an underexpanded rectangular jet in 3-D space. The rectangular nozzle protrudes into the computational domain by $l = 2D$, D being the width of the jet. The unstructured mesh consists of about 1.7 million tetrahedral cells. At the inlet plane, ambient (stationary) condition is specified. Jet flow at higher pressure is specified at the nozzle exit. All the rest boundaries are either Type I or Type II NRBC. Fig.s 14 shows snapshots of the isobars and v velocity contours on the cross sectional mid-planes after running 60,000 time steps. Fig. 15 demonstrates the 3-D pressure iso-surfaces. No visible reflection is observed.

3.5 Influence of the NRBC to the numerical accuracy

When the outflow boundary is non-reflecting, the influence from the boundary to the interior flow is small. Fig. 16 demonstrates the sound intensity level computed based on two domains with different lengths but same width for the 2-D Mach radiation problem in the 3rd CAA Workshop (Category 5) [16]. The short domain has a grid of 289 $\times$ 144 nodes. The only difference is that the longer domain has 30 more uniformly distributed nodes added in the x direction downstream. Fig. 16 shows the sound intensity levels (square of r.m.s. p' - pressure fluctuation) along the line $y = 10$ at $t = 400$ (40000 time steps or 28 periods) for both domains. It is observed that the maximum difference is about 2×10^{-10}, far below the discretization error, thus is negligible. This case also demonstrates the relative drifting side effect of the

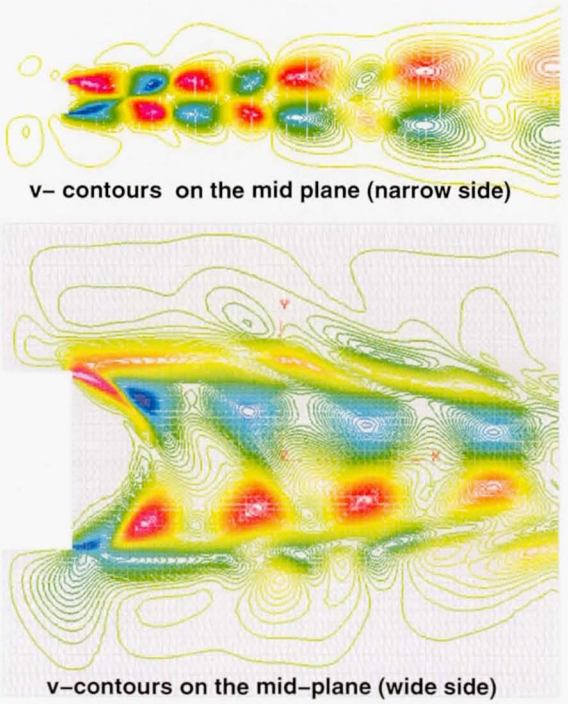

Figure 14: v velocity contours on the mid-planes with mesh background. No visible reflection is observed. At the outflow boundary, flow is supersonic in the jet core and then becomes subsonic across the thick shear layer.

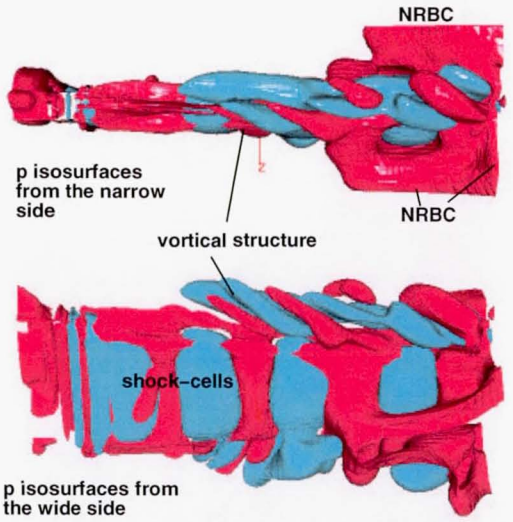

Figure 15: Pressure iso-surfaces, no reflection is observed.

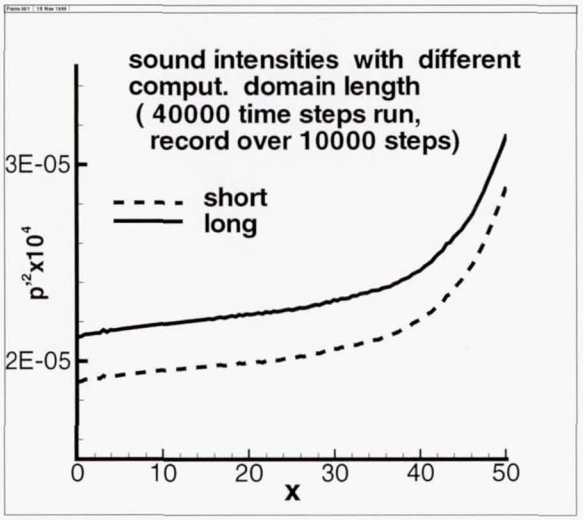

Figure 16: Comparison of sound intensity levels from computational domains of different lengths, showing that the outflow NRBC has negligible infuence to the interior.

extrapolation Type I NRBC, but the error is acceptable.

4 Numerical example for the absorbing boundary condition

As shown in §2.4, for an absorbing boundary condition such as the inlet, the prescribed inlet conditions are already good enough for an NRBC. Fig. 17 illustrates the instantaneous isobars for a cavity noise problem. $42,000$ triangulated structured cells are used. The problem is a M=0.8 flow past a cavity of aspect ratio of 6.5. At the cavity walls, no slip boundary condition is imposed. Due to vortex shedding and acoustic feedback at the cavity edges, strong nonlinear acoustic waves are generated and propagate in both upstream and downstream directions [15]. Fig. 18 is an enlargement of Fig. 17 around the inlet area. The details of the contours at the matched layer is revealed. It is observed that there is no spurious reflection and that the matched layer is about 4-5 cells' thick. The matched layer in the Type II NRBC is somewhat similar to that of the PML (perfectly matched layer) method [5,6] in that the difference diminishes quickly within this layer. But the layer arises automatically and there is no need to solve a new set of equations in the layer or to impose any conditions other than the prescribed inflow physical conditions.

For NRBC at the top of the computational domain, a Type I NRBC may be modified from (12) by simply exchanging the axes x and y: $\mathbf{U_Q} = \mathbf{U_P}, (\mathbf{U_y})_\mathbf{Q} = (\mathbf{U_x})_\mathbf{Q} = \mathbf{0}$, where as before, P and Q are respectively the boundary cell center and the ghost cell center at the top boundary. From Fig.s 17-18, even when the acoustic wave is oblique to the boundary, there is still no visible reflection. A Type I NRBC is applied to the outflow boundary, still, no visible reflection is found for the subsonic flow.

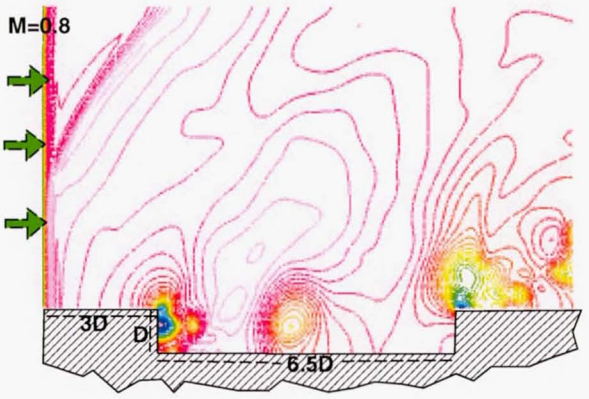

Figure 17: Isobars snapshot for a cavity noise problem (Mach number $M = 0.8$), showing inflow NRBC and its absorbing property. No visible reflection is found at the top and the outflow boundary

5 Application of the buffer/sponge zone

Generally, the NRBCs amount to very little reflection. However, there are situations that they may fail and discernible reflections occur. A simple but effective remedy is to add a buffer/sponge zone between the core domain and the boundary. In the buffer zone, the *same* governing equations are still used, except that the cell size in the buffer zone may grow rapidly (e.g. exponentially) and create larger numerical damping. Typically, the number of cells in a buffer zone may vary from a few to 20. An example of a 2-D axisymmetric jet with Mach radiation from an externally stimulated shear layer is demonstrated. It is similar to the one described in the 3rd CAA workshop benchmark problems (Category 5) [16]. The domain size is $33D \times 19D$ with D being the jet nozzle diameter. 300×280 non-uniform rectangular cells are used before they are further triangulated. Initially, a Mach number $M = 2$ jet exists. At the center of the nozzle exit plane, a source is imposed and perturbs the jet flow with a small amplitude $A = 0.001$ at a Strouhal number $St = 0.2$. Mach radiation is then triggered and gains its strength along the stream. At the outflow boundary, particularly at the shear layer, due to the staggered type mesh and the strong Mach waves, the Type I NRBC fails and spurious reflection is generated and propagates upstream (Fig. 19). After a buffer zone of 10 cells is added at the domain outflow boundary, the spurious reflection disappears and a clean mach wave radiation is shown (Fig. 20). The size of the buffer zone cells grows exponentially at a rate of 20% along the x axis.

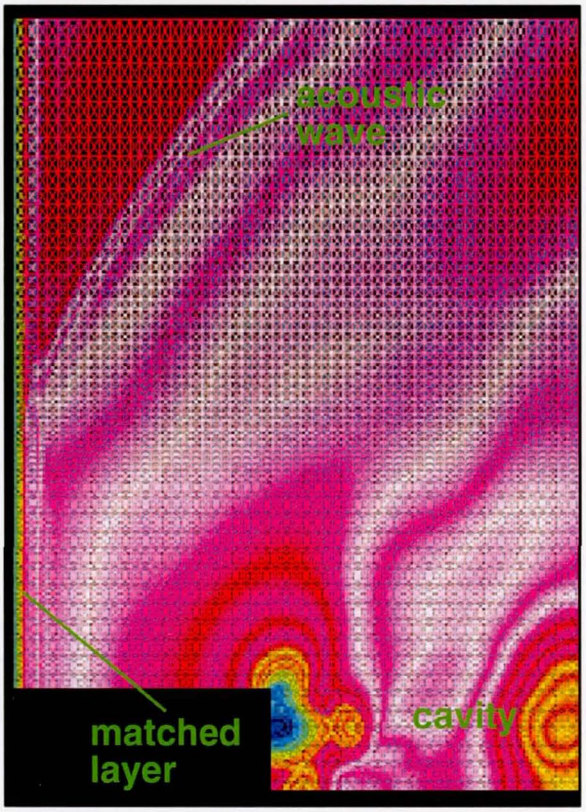

Figure 18: Details of the contours at the inflow boundary, showing the matched layer at the inlet and its spreading over the grid.

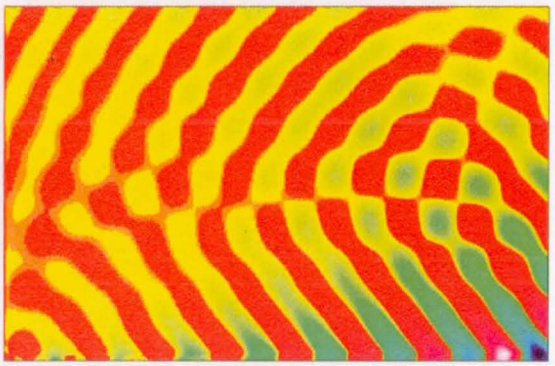

Figure 19: Mach radiation from a $M = 2$ axisymmetric jet (without buffer zone), showing severe spurious numerical reflection.

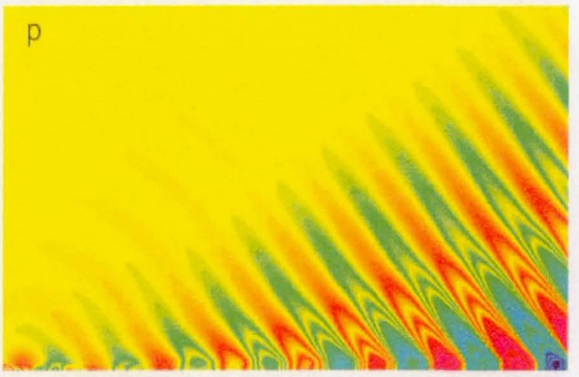

Figure 20: Mach radiation from a $M = 2$ axisymmetric jet (with buffer zone but not shown), showing a clean acoustic field.

6 Concluding Remarks

In the present paper, the hyperbolicity of the Euler equation system and the propagation of plane waves are revisited, and then combined to derive the continuity criterion of NRBC. The relation between flux balance across the boundary surface and the NRBC is established. Simple but effective C^1 continuity NRBCs are consequently developed.

These NRBCs are simple and robust, as demonstrated in the one and multi-dimensional numerical examples based on the the recent CE/SE method. Numerical examples with other finite volume schemes, e.g., N.T. (Nessyahu and Tadmor) or upwind schemes can be found in [17] (§8). Generally, their performances are similar to those of the characteristics-based NRBCs. Limitations of the NRBCs are also discussed in §2.5. In particular, the Type I extrapolation NRBCs may cause solution drifting due to lack of information beyond the (outflow) boundary. A remedy is to incorporate the physical boundary conditions or to use a sponge zone.

The diversity of various NRBCs in flow computations can never be overestimated. The purpose of the present paper is to show some guidelines in this direction and develop NRBCs that are simple but robust for practical computations. The compact updating procedure proves to work well with the NRBCs and provides C^1 accuracy in surface flux evaluation. But it is definitely not the *only* way to achieve non-reflecting effect. Different schemes may have different treatments. Sometimes, a combination of the NRBC treatments may provide much improved results, such as the incorporation of the buffer zone. As a byproduct, we are now able to explain why the NRBCs with the recently developed CE/SE scheme [10,11,14,15] are robust.

The restriction in §2.1 that the flow is continuous may be lifted, since for shock-capturing schemes, a discon-

tinuity may be considered as a continuous wave with steeper gradient. But if the wave propagation direction is oblique to the (artificial) boundary, the NRBC may perform poorly due to reasons explained in §2.5. Chang *et al* [9], Huynh [17] presented 1-D examples (i.e. wave propagation direction normal to the boundary) showing how a shock passes through an artificial boundary without causing visible reflection.

At last, we comment on the influence of the errors of the NRBCs on the accuracy for domain interior. Generally speaking, this involves the stability property of the scheme. If the time-marching explicit scheme satisfies the von Neumann stability criterion, an error introduced by the boundary condition will decay exponentially in time and space when it convects towards the domain interior.

Acknowledgements

This work received support from the Supersonic Propulsion Technology Project Office of NASA Glenn Research Center. The author wishes to thank Drs. R.Hixon, R. Blech, P.C.E. Jorgenson, A. Himansu and X.Y. Wang for fruitful discussions on the issues in the present paper.

References

[1] Courant, R. and Hilbert,D. " Methods of Mathematical Physics", Vol.II, John Wiley & Sons, London, 1962.

[2] Givoli,D., "Non-reflecting Boundary Conditions", *J. Comput. Phys.*, Vol. 94, 1-29(1991).

[3] Engquist, B. and Majda, A., "Absorbing boundary conditions for the numerical simulation of waves", *Math. Comp.*, Vol. 31, pp. 629-651 (1977).

[4] Thompson, K. W. "Time-dependent boundary conditions for hyperbolic systems", i & ii, *J. Comput. Phys.*, Vol. 68, pp. 1-24, (1987); also Vol 89, pp 439-461, (1990).

[5] Hu, F.Q., "On Absorbing Boundary Conditions for Linearized Euler Equations by a Perfectly Matched Layer", J. Comput. Phys., Vol.129, 201-219 (1996).

[6] Hesthaven, J.S.,"The Analysis and Construction of Perfectly Matched Layers for the Linearized Euler Equations", ICASE Report No. 97-49 (1997) (also in *J. Comput. Phys.*)

[7] Hedstrom,G.W., " Nonreflecting Boundary Conditions for Nonlinear Hyperbolic Systems", *J. Comput. Phys.* , Vol.30, 222-237 (1979).

[8] Hirsch, C. "Numerical Computation of Internal and External Flows" , Vol. II, John Wiley & Sons (1993).

[9] Chang, S. C., Himansu, A., Loh, C. Y., Wang, X. Y., Yu, S.-T. and Jorgenson, P. C. E. "Robust and Simple Non-Reflecting Boundary Conditions for the Space-Time Conservation Element and Solution Element Method ", AIAA Paper 97-2077 (1997).

[10] Chang, S. C., Wang, X. Y. and Chow, C. Y., " The Space-Time Conservation Element and Solution Element Method – A New High-Resolution and Genuine Multidimensional Paradigm for Solving Conservation Laws ", *J. Comput. Phys.* vol. 156, pp. 89-136 (1999).

[11] Wang, X.-Y. and Chang S.-C., " A 2-D Non-splitting Unstructured Triangular Mesh Euler Solver Based on the Space-Time Conservation Element and Solution Element Method" *CFD J.* vol. 8, pp309-325 (1999).

[12] Nessyahu, H. and Tadmor, E. "Non-oscillatory Central Diffewrencing for Hyperbolic Conservation Laws", *J. Comput. Phys.* , Vol.87, 408-463 (1990).

[13] "ICASE/LaRC Workshop on Benchmark Problems in Computational Aeroacoustics", Eds. J.Hardin, J.R.Ristorcelli, and C.K.W.Tam, NASA/CP-3300 (1994).

[14] Loh, C. Y., Hultgren, L. S. and Chang S.-C., "Computing Waves in Compressible Flow Using the Space-Time Conservation Element Solution Element Method," *AIAA J.*, Vol. 39, pp. 794-801 (2001).

[15] Loh, Ching Y., Wang, Xiao Y., Chang, Sin-Chung and Jorgenson, Philip C.E., "Computation of Feedback Aeroacoustic System by the CE/SE Method", in proceedings of the 1st Int'l Conf. on CFD (ICCFD), Kyoto, Japan, July, 2000; (published by Springer-Verlag, 2001).

[16] "Third Computational Aeroacoustics Workshop on Benchmark Problems", NASA/CP-2000-209790.

[17] Huynh, H.T., "Comparison and Improvement of Upwind and Centered Schemes on Quadrilateral and Triangular Meshes", AIAA Paper 2003-3541 (2003).

Appendix I: Plane wave solutions

The plane wave solutions are based on the Cauchy's method of Fourier Integral (see Courant and Hilbert[1], pp.210-211) for linear homogeneous differential equation. Consider Eq. (8):

$$\frac{\partial \mathbf{V}}{\partial t} + \tilde{A}\frac{\partial \mathbf{V}}{\partial x} + \tilde{B}\frac{\partial \mathbf{V}}{\partial y} + \tilde{C}\frac{\partial \mathbf{V}}{\partial z} = \tilde{\mathbf{Q}},$$

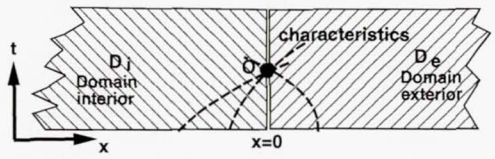

Figure 21: Continuity criterion in 1-D flow.

In the neighborhood of a point O ($\mathbf{x_0}$, t_0) at the artificial boundary, (8) can be locally linearized by setting the jacobians $\tilde{A}, \tilde{B}, \tilde{C}$ to their values at O. Assume a plane wave with the form $\mathbf{V} = \tilde{\mathbf{V}} e^{i\theta}$, and substitute in (8). Here $\theta = \theta(\mathbf{x}, t) = \mathbf{x} \bullet \mathbf{k} - \omega t$ is the phase of the simple wave, $i = \sqrt{-1}$. $\theta = const.$ stands for a characteristic surface or wave front [1]. (8) then becomes:

$$(\frac{\partial \tilde{\mathbf{V}}}{\partial t} + \tilde{A}\frac{\partial \tilde{\mathbf{V}}}{\partial x} + \tilde{B}\frac{\partial \tilde{\mathbf{V}}}{\partial y} + \tilde{C}\frac{\partial \tilde{\mathbf{V}}}{\partial z}) + i(\tilde{K} - \omega I)\tilde{\mathbf{V}} = \tilde{\mathbf{Q}} e^{-i\theta},$$

where I is the 5×5 identity matrix. For any given wave number vector $\mathbf{k} = (k_x, k_y, k_z)$, from the hyperbolicity of (8), real ωs exist such that $\tilde{K} - \omega I = 0$ (dispersion relation), where the matrix $\tilde{K} = k_x \tilde{A} + k_y \tilde{B} + k_z \tilde{C}$. Then the 'amplitude' $\tilde{\mathbf{V}}$ may be solved from

$$\frac{\partial \tilde{\mathbf{V}}}{\partial t} + \tilde{A}\frac{\partial \tilde{\mathbf{V}}}{\partial x} + \tilde{B}\frac{\partial \tilde{\mathbf{V}}}{\partial y} + \tilde{C}\frac{\partial \tilde{\mathbf{V}}}{\partial z} = \tilde{\mathbf{Q}} e^{-i\theta}$$

For more general waves other than the simple plane waves, as (8) is *locally* linearized in the neighborhood of the boundary point $O(\mathbf{x_0}, t_0)$, they may be decomposed by Fourier integral with respect to wave number $\mathbf{k}$ and replaced by the superposition of plane waves.

Appendix II: Discussions on the continuity criterion and the extrapolation technique

Without loss of generality, consider a 1-D flow shown in Fig. 21. As a pure initial value Cauchy problem, $\mathbf{V} = \mathbf{V}(x, 0)$ at $t = 0$ is given. This problem is well-posed and there exists a unique soluiton $\mathbf{V} = \mathbf{V}_o(x, t)$ over the entire domain D: $-\infty < x < \infty$, $t \geqslant 0$. If a boundary exists on the left inlet side, the problem becomes an initial-boundary-value problem, a boundary condition is required at the inlet boundary.

Assume the artificial boundary locates at $x = 0$ and bisects the entire domain D into domain interior D_i and domain exterior D_e: $D = D_i + D_e$ (see §2.1). In order that $\mathbf{V}_i$ and $\mathbf{V}_e$ in §2.1 are respectively the unique well-posed solutions in subdomains D_i and D_e, an admissible common boundary condition they share at $x = 0$ is:

$$\mathbf{V}_i(0, t) = \mathbf{V}_e(0, t) = \mathbf{V}_o(0, t).$$

Here, $\mathbf{V}_o(0, t)$ is the entire domain solution along the line $x = 0$; or equivalently, $\mathbf{V}_o(0, t)$ may be obtained by the method of characteristics as sketched in Fig. 21 at point O at the boundary.

However, for NRBC problems in reality, $\mathbf{V}_o(x, t)$, $x \geqslant 0$; or $\mathbf{V}_e(x, t)$ is totally missing (otherwise there is no need to investigate the NRBCs). In this situation, the extrapolation technique e.g. (12) is not an unreasonable choice for the NRBC continuity criterion. The initial-boundary value problem for $\mathbf{V}_i$ is well-posed only when the flow is supersonic or is known to remain unchanged across the artificial boundary at $x = 0$ by a priori information. Otherwise, even though *locally* the extrapolation (12) leads to non-reflecting effect, *globally* the 'solution' will keep drifting away and deviate from the true solution. The following are some remedies for practical numerical flow computations:

[1] use a sponge (buffer) zone with highly increased numerical damping to filter away the wave ingredients in the flow; when the Type I extrapolation NRBC is applied to the outer outflow boundary, the flow is already uniform at the boundary.

[2] incorporate the extrapolation with other physical boundary conditions (e.g. back pressure etc.).

Notice that the present discussions do not apply to the Type II NRBCs.